Azo–Hydrazone Tautomerism in Protonated Aminoazobenzenes: Resonance Raman Spectroscopy and Quantum-Chemical Calculations

ARTICLE *in* THE JOURNAL OF PHYSICAL CHEMISTRY A · JUNE 2008

Impact Factor: 2.69 · DOI: 10.1021/jp800217c · Source: PubMed

4 AUTHORS:

Deborah Matazo
University of São Paulo
2 PUBLICATIONS **38** CITATIONS
SEE PROFILE

Rômulo A Ando
University of São Paulo
67 PUBLICATIONS **529** CITATIONS
SEE PROFILE

Antonio Carlos Borin
University of São Paulo
75 PUBLICATIONS **1,435** CITATIONS
SEE PROFILE

Paulo S Santos
University of São Paulo
50 PUBLICATIONS **559** CITATIONS
SEE PROFILE

Azo−Hydrazone Tautomerism in Protonated Aminoazobenzenes: Resonance Raman Spectroscopy and Quantum-Chemical Calculations

Deborah R. C. Matazo, Rômulo A. Ando, Antonio C. Borin, and Paulo S. Santos*

Instituto de Química - USP//Instituto do Milênio de Materiais Complexos II, Av Lineu Prestes, 748 São Paulo, BR 05508-000, Brazil

Received: January 9, 2008; Revised Manuscript Received: February 20, 2008

The protonation effect on the vibrational and electronic spectra of 4-aminoazobenzene and 4-(dimethylamino)azobenzene was investigated by resonance Raman spectroscopy, and the results were discussed on the basis of quantum-chemical calculations. Although this class of molecular systems has been investigated in the past concerning the azo−hydrazone tautomerism, the present work is the first to use CASSCF/CASPT2 calculations to unveil the structure of both tautomers as well the nature of the molecular orbitals involved in chromophoric moieties responsible for the resonance Raman enhancement patterns. More specifically both the resonance Raman and theoretical results show clearly that in the neutral species, the charge transfer transition involves mainly the azo moiety, whereas in the protonated forms there is a great difference, depending on the tautomer. In fact, for the azo tautomer the transition is similar to that observed in the corresponding neutral species, whereas in the hydrazone tautomer such a transition is much more delocalized due to the contribution of the quinoid structure. The characterization of protonated species and the understanding of the tautomerization mechanism are crucial for controlling molecular properties depending on the polarity and pH of the medium.

Introduction

Azobenzene and its derivatives have been extensively investigated both experimentally and theoretically.[1–5] One of the reasons for such interest derives from their potential optically switchable properties, with the interconversion dynamics between the photostable states being the key for their use as molecular devices.[6–13] Substituted azobenzenes bearing an amino or dimethylamino group in the para position are well-known acid−base indicators, with the acidic form dark red colored as a consequence of the azo−hydrazone tautomerism in solution.[14–20] Aiming to understand the different charge distribution in such tautomers the present work was undertaken using resonance Raman spectroscopy to unveil the chromophoric moieties present, because each species absorbs in a rather distinct region of the visible−UV spectrum. Such information is central for the molecular design of aminoazobenzenes derivatives where one of the tautomers is preferentially present, with the consequent optimization of properties as optical nonlinearity, photoswitchability, and other molecular properties, depending on the chemical environment.

In fact, the azo−hydrazone (or ammonium−azonium) tautomerism, observed in protonated species of substituted azobenzene derivatives, was systematically studied by Jaffé et al. in 1950's on the basis of the UV−vis spectra,[14] and the main conclusion is that the high electronic delocalization can be assigned to the formation of a quinoid strucure in the hydrazone (azonium) tautomer. However, the characterization of both tautomers is of considerable controversy and many approaches are found in the literature, based on electronic absorption spectroscopy,[14–16] nuclear magnetic resonance NMR,[17] resonance Raman,[18–20] including semiempirical and *ab initio* calculations.[21]

SCHEME 1: Structures of the Neutral and Protonated 4-Amino (R = H) and 4-(Dimethylamino)azobenzene (R = CH_3), with the Corresponding Tautomeric Azo−Hydrazone Equilibrium

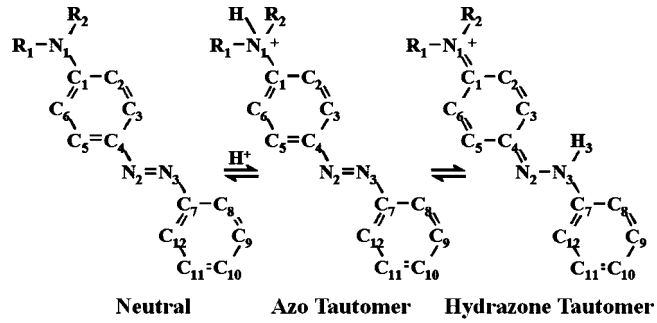

As a consequence of the substantial changes in the charge distribution of the excited electronic states, it is to be expected that azobenzene derivatives, as protonated amino- and (dimethylamino)azobenzene, display a particularly strong enhancement in their Raman spectra, showing the vibrational modes directly involved in the electronic excitation process. In fact, resonance Raman spectroscopy is the technique of choice to monitor the extent of the electronic delocalization in the chromophoric units of such molecules.

Although the hydrazone tautomer is well characterized, spectroscopic data of the azo (ammonium) tautomer are rare in the literature. To the best of our knowledge, there is not a systematic comparison between the tautomeric species, which motivated us to clarify several aspects of the subject. The present work provides a straightforward characterization of the tautomeric azo−hydrazone equilibrium employing UV−vis, resonance Raman spectroscopy and quantum-chemical calculations (CASSCF and CASPT2).[22] Particularly, the effect of the extra

* Corresponding author. Telephone number: 55-11-30913853. Fax number: 55-11-30913890. E-mail: pssantos@iq.usp.br.

10.1021/jp800217c CCC: $40.75
Published on Web 04/11/2008

TABLE 1: Calculated Interatomic Distances and Angles of Neutral 4-Aminoazobenzene and Respective Protonated Tautomeric Azo and Hydrazone Forms

bond	neutral	azo	hydrazone	bond	neutral	azo	hydrazone
				Distance/Å			
N_1-H_1	1.008	1.026	1.008	N_2-N_3	1.257	1.258	1.276
N_1-H_2	1.008	1.024	1.008	N_3-C_7	1.417	1.403	1.413
C_1-N_1	1.384	1.496	1.341	C_7-C_8	1.399	1.402	1.399
N_2-C_4	1.406	1.416	1.351	C_8-C_9	1.391	1.389	1.389
C_1-C_2	1.411	1.391	1.430	C_9-C_{10}	1.393	1.393	1.394
C_2-C_3	1.380	1.385	1.365	$C_{10}-C_{11}$	1.398	1.401	1.397
C_3-C_4	1.406	1.406	1.427	$C_{11}-C_{12}$	1.387	1.384	1.387
C_4-C_5	1.400	1.399	1.424	C_7-C_{12}	1.403	1.407	1.398
C_5-C_6	1.385	1.391	1.367	N_1-H_3		1.026	
C_1-C_6	1.406	1.386	1.420	N_3-H_3			1.002
				Angle/deg			
$H_1-N_1-H_2$	113.59	107.32	117.18	$C_4-N_2-N_3$	115.68	113.75	121.98
$C_1-N_1-H_1$	116.85	111.86	121.53	$N_2-N_3-C_7$	115.02	116.23	123.38
$C_1-N_1-H_2$	116.85	110.61	121.29	$N_3-C_7-C_8$	115.66	115.22	117.21
$N_1-C_1-C_2$	120.46	118.40	120.10	$N_3-C_7-C_{12}$	124.75	124.54	121.36
$N_1-C_1-C_6$	120.92	118.61	120.97	$C_7-C_8-C_9$	120.37	120.01	119.19
$N_2-C_4-C_5$	116.24	115.66	114.68	$C_8-C_9-C_{10}$	119.92	119.64	119.99
$N_2-C_4-C_3$	125.06	124.54	127.00	$C_9-C_{10}-C_{11}$	119.85	120.49	120.19
$C_1-C_2-C_3$	120.86	118.35	120.74	$C_{10}-C_{11}-C_{12}$	120.48	120.29	120.63
$C_2-C_3-C_4$	120.49	120.23	120.53	$C_{11}-C_{12}-C_7$	119.77	119.33	118.57
$C_3-C_4-C_5$	118.69	119.80	118.32	$C_8-C_7-C_{12}$	119.59	120.24	121.20
$C_4-C_5-C_6$	121.11	120.56	121.45	$H_1-N_1-H_3$		107.61	
$C_5-C_6-C_1$	120.29	118.07	120.03	$H_2-N_1-H_3$		107.32	
$C_6-C_1-C_2$	118.56	122.99	118.93	$N_2-N_3-H_3$			121.20

charge in the cations is discussed, comparing the resonance Raman enhancement patterns alongside with the calculated charge distribution in ground and excited electronic states.

Experimental Section

4-Aminoazobenzene ($C_{12}H_{11}N_3$ Aldrich, 98%) and 4-(dimethylamino)azobenzene ($C_{12}H_{15}N_3$, Sigma, 99%) were purchased from Aldrich and used without further purification. The solutions of the neutral species were obtained by direct dissolution in acetonitrile (CH_3CN Merck, 99.5%) and the protonated species were obtained by the addition of minute amounts of hydrochloric acid (HCl, Merck, 37%) in the respective CH_3CN solutions. The protonation process was monitored by UV−vis spectroscopy, as to reach a condition where only the monoprotonated species were present.[14] The UV−vis spectra of 10^{-4} M solutions were obtained in a Shimadzu UVPC 3010 using quartz cuvette cells of 1 mm of optical path. The respective Raman spectra, excited by several lines (351.1−514.5 nm) of an Ar^+ laser (Coherent INNOVA 90-6), were obtained in a Jobin-Yvon U1000 double spectrometer, with photomultiplier detection (Hamamatsu, RCA-A02 at −20 °C) using 90° signal collection configuration. The ca. 920 cm^{-1} Raman band of CH_3CN was used as the internal standard (spectral resolution 4 cm^{-1}). The laser beam was focused on the samples with ca. 25–50 mW of laser power and, to avoid local heating, the sample was contained in a small NMR tube coupled to a rotator shaft.

Theoretical Methods

The ground state geometries of the neutral species and of both tautomers of the protonated species (azo−hydrazone) were fully optimized employing the density functional theory (DFT) with the B3LYP[23] hybrid functional (Becke's gradient-corrected exchange correlation in conjunction with the Lee−Yang−Parr correlation functional with three parameters) and the 6-311G(d,p) one-electron atomic basis sets, without imposing geometric restrictions to the nuclear framework. Frequency analyses were carried out and no imaginary frequencies were found, indicating that the optimized geometries were in a minimum of the potential energy surface. Geometry optimizations were performed with the aid of the GAUSSIAN 03 software.[24]

TABLE 2: Experimental and Computed (CASPT2) Vertical Excitation Energies (E_{ver}), Related Oscillator Strengths (f), and CASSCF Dipole Moments (μ) for the Ground and Excited States of 4-Aminoazobenzene and Its Cation in the Azo and Hydrazone Tautomeric Forms

molecule	state	E_{ver} (eV)[a]	f	μ (D)	exp[a,b]
neutral	ground (S_0)			2.17	
	S_1 ($^1(n\pi^*)$)	3.56 (349)	0.0034	3.30	
	S_2 ($^1(\pi\pi^*)$)	3.83 (323)	0.9569	6.23	3.25 (382)
	S_3 ($^1(\pi\pi^*)$)	4.85 (255)	0.1087	6.11	4.96 (250)
	S_4 ($^1(\pi\pi^*)$)	5.04 (246)	0.0314	0.95	
azo	ground (S_0)			17.10	
	S_1 ($^1(n\pi^*)$)	3.20 (388)	0.0016	14.74	
	S_2 ($^1(\pi\pi^*)$)	3.92 (316)	0.6651	3.62	3.91 (317)
	S_3 ($^1(\pi\pi^*)$)	4.03 (307)	0.2164	5.37	
	S_4 ($^1(\pi\pi^*)$)	4.63 (268)	0.0097	17.97	
hydrazone	ground (S_0)			5.92	
	S_1 ($^1(\pi\pi^*)$)	2.76 (450)	1.3715	6.41	2.48 (500)
	S_2 ($^1(\pi\pi^*)$)	3.93 (315)	0.0150	6.02	
	S_3 ($^1(\pi\pi^*)$)	4.03 (307)	0.0151	9.98	
	S_4 ($^1(\pi\pi^*)$)	4.47 (277)	0.0029	2.56	

[a] Values in parenthesis are in nanometers. [b] Experimental values obtained in acetonitrile solution.

The vertical absorption electronic spectra were computed at the B3LYP optimized geometries employing the CASSCF/CASPT2 protocol (Complete Active Space (CAS) Self-Consistent Field (SCF) and Multiconfigurational Second-Order Perturbation (CASPT2),[22] which has been successfully employed for describing spectroscopic properties of different kinds of compounds.[25–29] Following a similar procedure adopted by us previously,[28,29] double-ζ with polarization ANO basis sets (atomic natural orbital (ANO)[30] were employed for describing the carbon, nitrogen, and oxygen atoms. The shifted zero-order

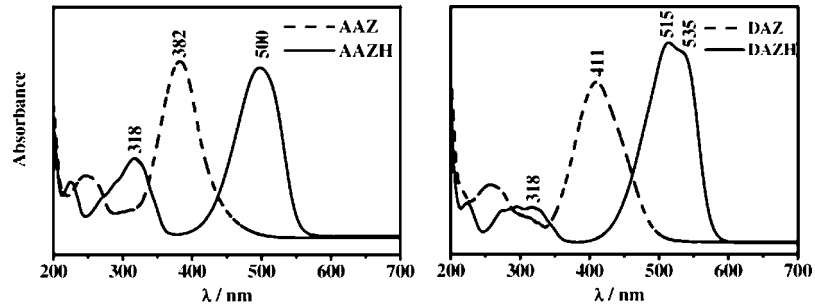

Figure 1. Electronic spectra of 4-amino- (AAZ) and 4-(dimethylamino)azobenzene (DAZ) in neutral and acidic (AAZH and DAZH) acetonitrile solutions.

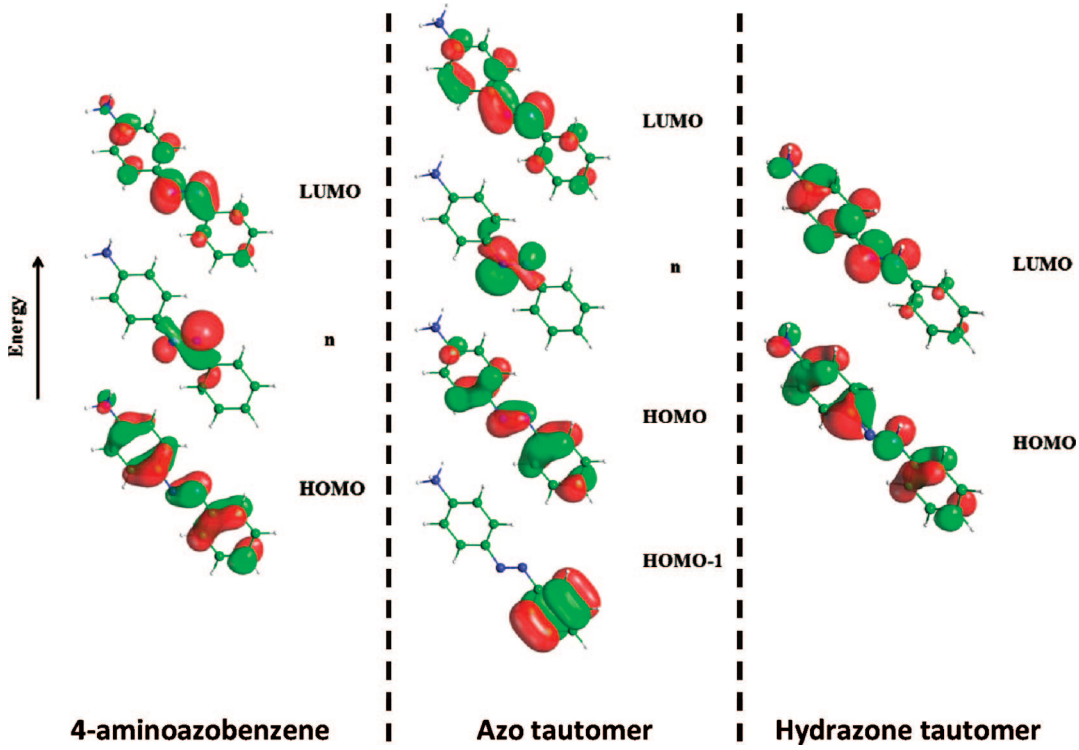

Figure 2. Contours of the molecular orbitals involved in the electronic transitions of the neutral 4-aminoazobenzene and protonated tautomeric azo and hydrazone species.

Hamiltonian proposed by Ghigo, Roos, and Malmqvist[31] (shift parameter of 0.25 Hartree) was used for the CASPT2 calculations. Intruder states interacting weakly with the reference functions were removed with an imaginary level shift of 0.1 au.[32] The CASSCF/CASPT2 calculations were carried out with the MOLCAS 6.4 software.[33]

The active spaces were built on the basis of the analysis of a series of test calculations, from which we concluded that for computing the low-lying excited states of $\pi-\pi^*$ and $n-\pi^*$ character a CASSCF (12, 12), that is distributing 12 electrons in 12 molecular orbitals comprising the most relevant n, π, and π^* molecular orbitals, is sufficient. The reference functions for the ground and excited $^1(\pi\pi^*)$ and $^1(n\pi^*)$ electronic states were obtained from average CASSCF calculations, including in the averaging the ground, the first three lowest-lying $^1(\pi\pi^*)$ plus one $^1(n\pi^*)$ electronic state (five roots in total). Core orbitals were kept frozen in the form determined by the ground state closed-shell Hartree-Fock wave function, at both CASSCF and CASPT2 steps. Oscillator strengths (f) were computed by combining the transition dipole moments (TDM) from the ground to the excited states, computed from the CASSCF wave functions obtained as described above with the aid of the CASSCF state interaction (CASSI) method,[34] and the vertical transition energies obtained at the CASPT2 level.

Results and Discussion

In Scheme 1 are shown the structures of the investigated species in neutral (4-aminoazobenzene, AAZ and 4-(dimethylamino)azobenzene, DAZ) and cationic forms (AAZH and DAZH, respectively), and the corresponding tautomeric equilibria (azo−hydrazone) for the protonated species. In the hydrazone tautomer (Scheme 1) the proton is located in N_3 on the basis of X-ray investigation[35] and quantum-chemical calculations.[21] In Table 1 are displayed the calculated interatomic distances and angles for the respective structures of 4-aminoazobenzene.

The bond length changes (Table 1) show a clear agreement with the structures proposed in Scheme 1, because there are modest variations comparing the neutral AAZ structure with the azo form of AAZH, whereas for the hydrazone tautomer there is a substantial shortening of the N_2-C_4 and C_2-C_3 (C_5-C_6) bonds, concomitantly with the elongation of the N_2-N_3 bond, indicating clearly the quinoid structure on the amino substituted ring.

TABLE 3: Mulliken Charges for Individual Atoms in 4-Aminoazobenzene and in Tautomeric Forms (Azo−Hydrazone) of the Protonated Species in Ground (S_0) and Most Relevant Excited Electronic States

	electronic states		
atom	neutral S_0/S_2	azo S_0/S_2	hydrazone S_0/S_1
H_1	0.8691/0.1315	0.1140/0.1117	0.1582/0.1586
H_2	0.8689/0.1318	0.1117/0.1093	0.1567/0.1572
H_3		0.2117/0.2117	0.1621/0.1578
N_1	−0.2861/−0.2649	0.1184/0.1155	−0.1878/−0.1644
C_1	0.3440/0.3824	0.2883/0.2062	0.3931/0.4020
C_2	−0.1569/−0.1287	−0.1451/−0.1693	−0.1008/−0.0979
C_3	−0.1067/−0.1044	−0.0694/−0.1353	−0.1168/−0.1357
C_4	0.1200/0.3006	0.2192/0.1888	0.1053/0.1528
C_5	−0.0302/−0.0114	−0.0017/−0.0353	0.0372/0.0035
C_6	−0.1684/−0.1328	−0.1195/−0.1820	−0.1267/−0.1003
N_2	−0.2364/−0.4169	−0.2800/−0.3896	−0.1831/−0.2283
N_3	−0.2361/−0.4629	−0.2023/−0.3519	−0.0465/−0.1346
C_7	0.1607/0.2317	0.1275/0.3269	0.2406/0.3120
C_8	−0.0696/−0.0717	−0.0638/−0.0359	−0.1130/−0.1081
C_9	−0.0291/−0.0272	−0.0241/0.0572	−0.0111/−0.0039
C_{10}	−0.0318/−0.0441	−0.0109/0.0536	−0.0085/−0.0020
C_{11}	−0.0254/−0.0240	−0.0188/−0.0016	−0.0063/−0.0085
C_{12}	−0.1567/−0.1622	−0.1535/0.0203	−0.1622/−0.1688

The UV−vis spectra of AAZ and DAZ dissolved in neat CH_3CN and in CH_3CN containing HCl are shown in Figure 1, making obvious the substantial shifts in the λ_{max} after protonation. In fact, Figure 1 reveals that a tautomeric equilibrium is present, with the band at ca. 320 nm being assigned to the azo form, and the band at ca. 500 nm being assigned to the hydrazone form of AAZH. For DAZH the corresponding values are red shifted by ca. 30 and 20 nm, respectively. In both cases, the displacement of the electronic transitions to the red in the hydrazone tautomer, comparatively to the azo tautomer, can be rationalized by the quinoid structure of the former, which is a more π delocalized structure. On the other hand the slight red shift observed in the hydrazone tautomer of DAZH compared to AAZH, can be understood in terms of the stronger electron donor properties of the $N(CH_3)_2$ substituent, given the induction effect of the methyl groups.

The experimental excitation energies obtained in acetonitrile solution and the values of the calculated vertical transition energies are reported in Table 2, together with the dipole moments for ground (S_0) and excited states (S_n, where $n = 1$–4) for the neutral and cationic species. It must be remembered that the quantum chemical calculations were performed in vacuum (gas phase) and the discrepancies with experimental values (CH_3CN solution) are acceptable. The most relevant molecular orbitals involved in the lowest energy electronic transitions are plotted in Figure 2.

For the neutral species, the CASSCF/CASPT2 results (Table 2) predict the lowest excited electronic state (S_1) as a $^1(n\pi^*)$, located at 3.56 eV (349 nm), with dipole moment of $\mu(S_1) = 3.30$ D, and $\mu(S_0) = 2.17$ D for the ground state. As expected, the electronic transition from the ground (S_0) to the S_1 state is weak, with a computed oscillator strength of $f(S_1 \leftarrow S_0) =$

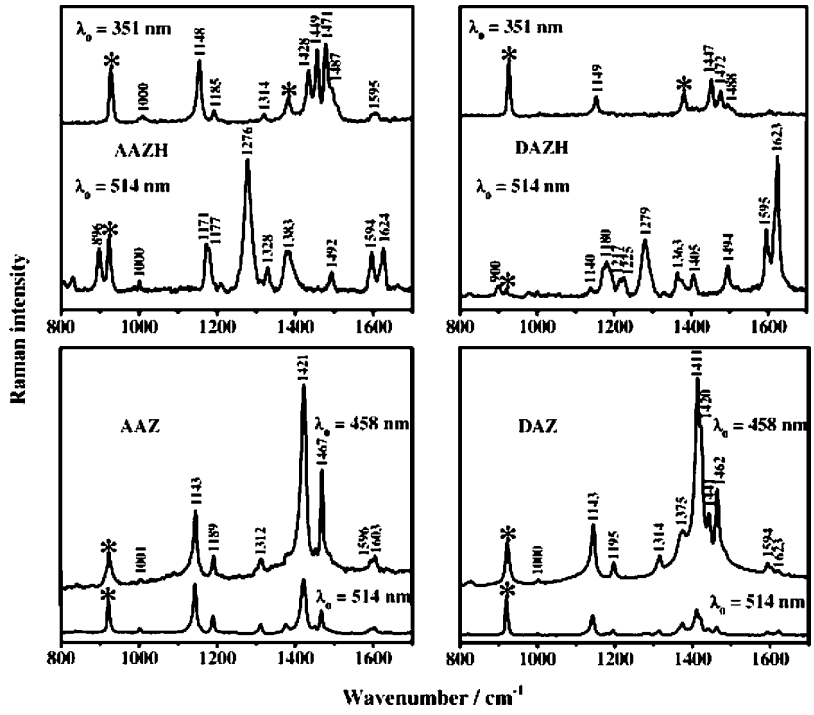

Figure 3. Raman spectra of neutral and cationic species of 4-amino- (AAZ/AAZH) and 4-(dimethylamino)azobenzene (DAZ/DAZH) in acetonitrile solutions at different excitation energies. Internal standard is at 920 cm^{-1} (CH_3CN).

TABLE 4: Experimental and Calculated Raman Frequencies with Corresponding Assignments for the Main Vibrational Modes of 4-Aminoazobenzene in Neutral Form and Protonated Tautomers (Azo and Hydrazone)

4-aminoazobenzene			azo tautomer			hydrazone tautomer		
exp	calc	assignment	exp	calc	assignment	exp	calc	assignment
						896	906	δ(N−N), ϕ(1)
1001	1015	ϕ(12)	1000	1015	ϕ(12)	1000	1014	ϕ(12)
1143	1145	ν(C−N_{AZO}), δ(C−H)	1148	1157	ν(C−N_{AZO}), δ(C−H)			
						1171		δ(C−H)
1189		δ(C−H)	1185		δ(C−H)	1177		δ(C−H)
						1276	1226	ν(C−N_{AZO}), δ(C−H)
1312	1321	δ(C−H), ν(C−NH_2)	1314	1328	δ(C−H)	1328	1314	δ(C−H), ν(N−N)
						1383	1390	γ(NH_2), ϕ(18b)
1421		ν(N═N)	1428		ν(N═N)			
			1449	1449	ν(N═N), δ(C−H)			
1467	1468	ν(N═N), δ(C−H)	1471	1479	δ(C−H), ν(N═N)			
			1487			1492	1489	δ(C−H)
1596			1595	1617	ϕ(8a)	1594	1594	ϕ(8a), ν(N−N)
1603	1609	ϕ(8a)				1624	1630	ϕ(8a)

0.0034. The next singlet excited state (S_2), located at 3.83 eV (323 nm), is a $^1(\pi\pi^*)$ state with a dipole moment of $\mu(S_2) = 6.23$ D. The S_2 state carries most of the intensity, with oscillator strength of $f(S_2 \leftarrow S_0) = 0.9569$. Therefore, the strongest electronic absorption band observed experimentally at 3.25 eV (382 nm) can be assigned to the $S_2 \leftarrow S_0$ ($\pi\pi^*$) electronic transition. On the basis of the population analysis of the natural orbitals (NO) of the CASSCF wave function, the S_2 state derives from the ground (S_0) state by a one-electron excitation from the highest-lying occupied NO (HOMO-like) to the lowest-lying unoccupied NO (LUMO-like), being the CASSCF wave function dominated by one single configuration (weight in parenthesis): HOMO-like → LUMO-like (77%). The vertical $S_2 \leftarrow S_0$ ($\pi\pi^*$) electronic transition is associated with a transfer of electron density to the azo moiety (Figure 2, 4-aminoazobenzene). This charge reorganization correlates nicely with the variation of the corresponding Mulliken atomic charges (Table 3), which for the azo moiety N atoms go from −0.2364 and −0.2631 (N_2 and N_3, respectively) in the ground state to −0.4169 and −0.4629 (N_2 and N_3, respectively) in the excited (S_2) state. It can be observed the presence of other two $^1(\pi\pi^*)$ excited states (Table 2). The S_3 electronic state is located at 4.85 eV (255 nm) and is dominated by the HOMO−1-like → LUMO (81%) excited configuration, with a dipole moment of $\mu(S_3) = 6.11$ D, and oscillator strength of $f(S_3 \leftarrow S_0) = 0.1087$. It is worth mentioning that a weak band is observed experimentally at 4.96 eV (250 nm), which can be assigned to the $S_3 \leftarrow S_0$ vertical electronic transition computed by us. Finally, the S_4 excited state is located 5.04 eV (246 nm), with a dipole moment of $\mu(S_4) = 0.95$ D, and being described by the HOMO−2-like → LUMO (46%) electronic configuration. The $S_4 \leftarrow S_0$ vertical electronic transition is very weak, with computed oscillator strength of $f(S_4 \leftarrow S_0) = 0.0314$.

Considering now the protonated species, the lowest-lying electronic state (S_1) of the azo tautomer is located at 3.20 eV (388 nm) and the largest contribution to the wavefunction stems from the single promotion n → LUMO-like (76%) (Figure 2, azo), characterizing it as a $^1(n\pi^*)$ electronic state. The dipole moment of the azo S_1 electronic state is $\mu(S_1) = 14.74$ D, in comparison to $\mu(S_0) = 17.10$ D for the ground state; the corresponding $S_1 \leftarrow S_0$ vertical electronic transition is weak ($f(S_1 \leftarrow S_0) = 0.0016$). The S_2 electronic state carries most of the intensity, $f(S_2 \leftarrow S_0) = 0.6651$, and it is located at 3.92 eV (316 nm), with a dipole moment of $\mu(S_2) = 3.62$ D, and the wavefunction dominated by a single electronic configuration, best represented by the promotion HOMO-like → LUMO-like (64%); therefore, the S_2 state is a $^1(\pi\pi^*)$ valence electronic state. The $S_2 \leftarrow S_0$ vertical electronic transition involves charge reorganization, with electrons being transferred to the azo moiety, for which the Mulliken atomic charges go from −0.2800 and −0.2023 (N_2 and N_3, respectively) in the ground state to −0.3896 and −0.3519 (N_2 and N_3, respectively) in the S_2 state (Table 3). This behavior is similar to that for the analogous electronic transition in the neutral 4-aminoazobenzene species. The next $^1(\pi\pi^*)$ excited state (S_3) is located at 4.03 eV (307 nm), with a dipole moment of $\mu(S_3) = 5.37$ D, with an associated $S_3 \leftarrow S_0$ oscillator strength of $f(S_3 \leftarrow S_0) = 0.2164$, with the electronic wavefunction dominated by the configuration HOMO−1-like → LUMO-like (66%). The highest $^1(\pi\pi^*)$ excited state (S_4) computed by us is located at 4.63 eV (268 nm), with a dipole moment of $\mu(S_4) = 17.97$ D, and an oscillator strength associated to the $S_4 \leftarrow S_0$ transition, very small $f(S_4 \leftarrow S_0) = 0.0097$.

The CASSCF/CASPT2 results for the hydrazone tautomer (Table 2), show a very strong electronic transition ($S_1 \leftarrow S_0$, $f = 1.3715$). The S_1 excited state, $^1(\pi\pi^*)$ is located at 2.76 eV (450 nm), with a dipole moment of $\mu(S_1) = 6.41$ D, compared to $\mu(S_0) = 5.92$ D for the ground state. The wavefunction for the S_1 excited state is dominated by a single configuration, derived from the ground state by the HOMO-like → LUMO-like (73%) single excitation (Figure 2, hydrazone). As before, the $S_1 \leftarrow S_0$ vertical excitation is followed by a charge transfer to the azo moiety, with the corresponding Mulliken atomic charges for the corresponding N atoms varying from −0.1831 and −0.0465 (N_2 and N_3, respectively) in the S_0 state to −0.2283 and −0.1346 (N_2 and N_3, respectively) in the S_1 excited state.

After presenting the results for both tautomeric forms individually, it is worth comparing the computed to the experimental UV−vis spectra. Experimentally, two bands are observed, a strong one at 2.48 eV (500 nm) followed by a weaker band at 3.91 eV (317 nm). According to our CASSCF/CASPT2 results (Table 2) the strongest electronic band can be assigned to the $S_1 \leftarrow S_0$ electronic transition in the hydrazone tautomer, which is theoretically predicted at 2.76 eV (450 nm), compared to the experimental value of 2.48 eV (500 nm). The weaker one can be assigned to the $S_2 \leftarrow S_0$ electronic transition of the azo tautomer, predicted theoretically at 3.92 eV (316 nm), compared to the experimental value of 3.91 eV (317 nm). The $S_3 \leftarrow S_0$ transition, located theoretically at 4.03 eV (307 nm) with a smaller oscillator strength $f(S_3 \leftarrow S_0) = 0.2164$ than that corresponding to the $S_1 \leftarrow S_0$ one, $f(S_1 \leftarrow S_0) = 0.6651$, can also contribute to the experimentally observed band centered

at 3.91 eV (317 nm). Furthermore, the experimental gap between the two bands is about 1.4 eV, and the computed gap amounts to 1.2 eV. By the analysis carried out above, one can conclude that the bands observed experimentally are due to the simultaneous presence of both tautomers in the acidic solution, because the computed results suggest that such species have strong transition at rather different energies of the spectra.

The Raman spectra of neutral, AAZ and DAZ, and the protonated species, AAZH and DAZH, for different excitation energies are shown in Figure 3, and Table 4 displays the experimental and calculated Raman frequencies for the more relevant vibrational modes, with the corresponding assignments. In Figure 3 (AAZ and DAZ) are displayed the well studied neutral species resonance Raman spectra (AAZ and DAZ), with the strong enhancement of ν(N═N) and ν(C−N) at ca. 1421 and 1143 cm^{-1}, respectively. Such results are in line with the calculated Mulliken charges for individual atoms shown in Table 3, because there is a significant variation in the charge of N_2 and N_3 atoms between ground (S_0) and excited (S_2) state.

The quantum-chemical calculations indicate that in acidic solutions both tautomers are present and are experimentally observed with the right choice of the wavelength by their resonance Raman enhancement patterns as seen in Figure 3 (AAZH and DAZH). The Raman spectrum of AAZH excited at $\lambda_0 = 514$ nm, reveals the selective enhancement of modes at ca. 1171, 1276, 1594 and 1624 cm^{-1}, easily assigned to δ(C−H), ν(C−N), $\phi(8a)_{benzenoid}$ and $\phi(8a)_{quinoid}$, respectively, revealing the hydrazone tautomer. On the other hand, the spectrum excited at $\lambda_0 = 351$ nm reveals the azo tautomer, in a rather selective way, whereas the enhancement of modes with great participation of ν(N═N) and $\nu(C-N_{azo})$ are observed at ca. 1450 and 1148 cm^{-1}, respectively. The resonance Raman profile of DAZH reveals the same kind of behavior, although in this case, excited at $\lambda_0 = 514$ nm; the vibrational modes at ca. 1595 and 1623 cm^{-1} assigned to ring modes are even more enhanced compared to the other modes, which evidences the greater participation of the quinoid ring in the chromophore, a consequence of the stronger electron donor character of the dimethyl-amino substituent.

Conclusion

Resonance Raman spectroscopy and quantum chemical calculations of 4-aminoazobenzene and 4-(dimethylamino)-azobenzene and the respective cations have proved in a definite way the presence of the tautomeric (azo−hydrazone) equilibria in the protonated species. The quantum-chemical calculations reveal rather interesting features of the different tautomers; more specifically, a huge difference in the electronic dipole moments in the ground and excited states. In addition, such calculations also reveal a much greater extent of charge transfer to the N═N group in the case of the azo tautomer, because in the case of the hydrazone tautomer the electronic structure is much more delocalized, which is in line with observed electronic and resonance Raman spectra. It is worth mentioning that the azo−hydrazone tautomerism present in the investigated species can be selectively displaced toward one of the forms by the solvent polarity and pH of the medium, which opens an interesting possibility for the use of such systems in molecular systems that present several microdomains of different polarities and local pHs, as is the case of ionic liquids, zeolites, layered materials, etc.

Acknowledgment. We acknowledge FAPESP (Fundação de Amparo à Pesquisa do Estado de São Paulo), CNPq (Conselho Nacional de Desenvolvimento Cientiíico and Tecnológico), and IMMC (Instituto do Milênio de Materiais Complexos II). A.C.B. acknowledges computer time from the Laboratório de Computação Científica Avançada da Universidade de São Paulo. We are grateful thank to Prof. Dr. Oswaldo Sala for his assistance in acquiring the Raman spectra excited in the UV ($\lambda_0 = 351$ nm).

References and Notes

(1) Zimmerman, G.; Chow, L. Y.; Paik, U. J. *J. Am. Chem. Soc.* **1958**, *80*, 3528.
(2) Beveridg, D. L.; Jaffe, H. H. *J. Am. Chem. Soc.* **1966**, *88*, 1948.
(3) Griffith, J. *Chem. Soc. Rev.* **1972**, *1*, 481.
(4) Fliegl, H.; Kohn, A.; Hattig, C.; Ahlrichs, R. *J. Am. Chem. Soc.* **2003**, *125*, 9821.
(5) (a) Biswas, N.; Umapathy, S. *J. Phys. Chem. A* **1997**, *101*, 5555. (b) Biswas, N.; Umapathy, S. *J. Phys. Chem A* **2000**, *104*, 2734. (c) Biswas, N.; Umapathy, S. *J. Raman Spectrosc.* **2001**, *32*, 471. (d) Biswas, N.; Abraham, B.; Umapathy, S. *J. Phys. Chem. A* **2002**, *106*, 9397. (e) Biswas, N.; Umapathy, S. *J. Chem. Phys.* **2003**, *118*, 5526.
(6) Kumar, G. S.; Neckers, D. C. *Chem. Rev.* **1989**, *89*, 1915.
(7) Liu, Z. F.; Hashimoto, K.; Fujishima, A. *Nature* **1990**, *347*, 658.
(8) Ikeda, T.; Tsutsumi, O. *Science* **1995**, *268*, 1873.
(9) Archut, A.; Vogtle, F.; De Cola, L.; Azzellini, G. C.; Balzani, V.; Ramanujam, P. S.; Berg, R. H. *Chem.-Eur. J.* **1998**, *4*, 699.
(10) Natansohn, A.; Rochon, P. *Adv. Mater.* **1999**, *11*, 1387.
(11) Natansohn, A.; Rochon, P. *Chem. Rev.* **2002**, *102*, 4139.
(12) Yagai, S.; Karatsu, T.; Kitamura, A. *Chem.-Eur. J.* **2005**, *11*, 4054.
(13) Antonov, L.; Kamada, K.; Nedeltcheva, D.; Ohta, K.; Kamounah, F. S. *J. Photochem. Photobiol. A-Chem.* **2006**, *181*, 274.
(14) (a) Jaffe, H. H.; Yeh, S. J. *J. Org. Chem.* **1957**, *22*, 1281. (b) Jaffe, H. H.; Gardner, R. W. *J. Am. Chem. Soc.* **1958**, *80*, 319. (c) Yeh, S. J.; Jaffe, H. H. *J. Am. Chem. Soc.* **1959**, *81*, 3279. (d) Yeh, S. J.; Jaffe, H. H. *J. Am. Chem. Soc.* **1959**, *81*, 3283. (e) Isaks, M.; Jaffe, H. H. *J. Am. Chem. Soc.* **1964**, *86*, 2209. (f) Jaffe, H. H.; Yeh, S. J.; Gardner, R. W. *J. Mol. Spectrosc.* **1958**, *2*, 120.
(15) Klotz, I. M.; Fiess, H. A.; Ho, J. Y. C.; Mellody, M. *J. Am. Chem. Soc.* **1954**, *76*, 5136.
(16) Cilento, G.; Miller, E. C.; Miller, J. A. *J. Am. Chem. Soc.* **1956**, *78*, 1718.
(17) Kuroda, Y.; Lee, H.; Kuwae, A. *J. Phys. Chem.* **1980**, *84*, 3417.
(18) (a) Machida, K.; Kim, B. K.; Saito, Y.; Igarashi, K.; Uno, T. *Bull. Chem. Soc. Jpn.* **1974**, *47*, 78. (b) Uno, T.; Kim, B. K.; Saito, Y.; Machida, K. *Spectroc. Acta Pt. A-Mol. Biomol. Spectrosc.* **1976**, *32*, 1179. (c) Machida, K. *Resonance Raman Spectra and Protonation Equilibria of Azo Dyes*; Bist, H. D., Durig J. R., Sullivan, J. F., Eds.; Raman Spectroscopy: Sixty Years on Vibrational Spectra and Structure, Vol. 17A; Publisher: Location of Publisher, 1989; pp 421–442.
(19) Bell, S.; Bisset, A.; Dines, T. J. *J. Raman Spectrosc.* **1998**, *29*, 447.
(20) Dines, T. J.; MacGregor, L. D.; Rochester, C. H. *Chem. Phys.* **2006**, *322*, 445.
(21) Liwo, A.; Tempczyk, A.; Widernik, T.; Klentak, T.; Czerminski, J. *J. Chem. Soc.-Perkin Trans. 2* **1994**, *2*, 71.
(22) (a) Roos, B. O. *In Advances in Chemical Physics; Ab Initio Methods in Quantum Chemistry - II*; Lawley, K. P., Ed.; John Wiley & Sons: Chichester, 1987; (b) Andersson, K.; Malmqvist, P. A.; Roos, B. O.; Sadlej, A. J.; Wolinski, K. *J. Phys. Chem.* **1990**, *94*, 5483. (c) Andersson, K.; Malmqvist, P. A.; Roos, B. O. *J. Chem. Phys.* **1992**, *96*, 1218.
(23) (a) Becke, A. D. *J. Chem. Phys.* **1993**, *98*, 5648. (b) Lee, C. T.; Yang, W.; Parr, R. G. *Phys. Rev. B* **1988**, *37*, 785. (c) Stephens, P. J.; Devlin, F. J.; Chabalowski, C. F.; Frish, M. J. *J. Phys. Chem.* **1994**, *98*, 11623.
(24) Frisch, M. J.; Trucks, G. W.; Schlegel, H. B.; Scuseria, G. E.; Robb, M. A.; Cheeseman, J. R.; Montgomery, J. A., Jr.; Vreven, T.; Kudin, K. N.; Burant, J. C.; Millam, J. M.; Iyengar, S. S.; Tomasi, J.; Barone, V.; Mennucci, B.; Cossi, M.; Scalmani, G.; Rega, N.; Petersson, G. A.; Nakatsuji, H.; Hada, M.; Ehara, M.; Toyota, K.; Fukuda, R.; Hasegawa, J.; Ishida, M.; Nakajima, T.; Honda, Y.; Kitao, O.; Nakai, H.; Klene, M.; Li, X.; Knox, J. E.; Hratchian, H. P.; Cross, J. B.; Bakken, V.; Adamo, C.; Jaramillo, J.; Gomperts, R.; Stratmann, R. E.; Yazyev, O.; Austin, A. J.; Cammi, R.; Pomelli, C.; Ochterski, J. W.; Ayala, P. Y.; Morokuma, K.; Voth, G. A.; Salvador, P.; Dannenberg, J. J.; Zakrzewski, V. G.; Dapprich, S.; Daniels, A. D.; Strain, M. C.; Farkas, O.; Malick, D. K.; Rabuck, A. D.; Raghavachari, K.; Foresman, J. B.; Ortiz, J. V.; Cui, Q.; Baboul, A. G.; Clifford, S.; Cioslowski, J.; Stefanov, B. B.; Liu, G.; Liashenko, A.; Piskorz, P.; Komaromi, I.; Martin, R. L.; Fox, D. J.; Keith, T.; Al-Laham, M. A.; Peng, C. Y.; Nanayakkara, A.; Challacombe, M.; Gill, P. M. W.; Johnson, B.; Chen, W.; Wong, M. W.; Gonzalez, C.; Pople, J. A. *Gaussian 03*, revision D.01;Gaussian, Inc.: Wallingford, CT, 2004.

(25) Roos, B. O.; Fülscher, M. P.; Malmqvist, P. A.; Merchán, M.; Serrano-Andrés, L. *Quantum Mechanical Electronic Structure Calculations with Chemical Accuracy*; Langhoff, S. R., Ed.; Kluwer Academic: Dordrecht, The Netherlands, 1995.

(26) Roos, B. O.; Borin, A. C.; Gagliardi, L. *Angew. Chem. Int. Ed.* **2007**, *46*, 1469.

(27) Serrano-Andrés, L.; Merchán, M.; Borin, A. C. *Proc. Nat. Acad. Sci.* **2006**, *103*, 8691.

(28) Ando, R. A.; Borin, A. C.; Santos, P. S. *J. Phys. Chem A* **2007**, *111*, 7194.

(29) Ando, R. A.; Rodríguez-Redondo, J. L.; Sastre-Santos, A.; Fernández-Lázaro, F.; Azzellini, G. C.; Borin, A. C.; Santos, P. S. *J. Phys. Chem A* **2007**, *111*, 13452.

(30) Widmark, P. O.; Malmqvist, P. A.; Roos, B. O. *Theor. Chim. Acta* **1990**, *77*, 291.

(31) Ghigo, G.; Roos, B. O.; Malmqvist, P. A. *Chem. Phys. Lett.* **2004**, *396*, 142.

(32) Forsberg, N.; Malmqvist, P. A. *Chem. Phys. Lett.* **1997**, *274*, 196.

(33) Karlström, G.; Lindh, R.; Malmqvist, P. A.; Roos, B. O.; Ryde, U.; Veryazov, V.; Widmark, P. O.; Cossi, M.; Schimmelpfennig, B.; Neogrady, P.; Seijo, L. *Comput. Mater. Sci.* **2003**, *28*, 222.

(34) (a) Malmqvist, P. A. *Int. J. Quantum Chem.* **1986**, *30*, 479. (b) Malmqvist, P. A.; Roos, B. O. *Chem. Phys. Lett.* **1989**, *155*, 189.

(35) Yatsenko, A. V.; Chernyshev, V. V.; Kurbakov, A. I.; Schenk, H. *Acta Crystallogr. Sect. C-Cryst. Struct. Commun.* **2000**, *56*, 892.

JP800217C